Dynamic interaction analysis of actively controlled maglev vehicles and guideway girders considering nonlinear electromagnetic forces

Dong-Ju Min[1], Jun-Seok Lee[2] and Moon-Young Kim*[1]

[1]*Department of Civil and Environmental Engineering, Sungkyunkwan University, Cheoncheon-Dong, Jangan-gu, Suwon 440-746, S. Korea*
[2]*Civil Engineering Team, Samsung C&T Corporation, Seoch02-Dong, Seocho-Gu, Seoul 137-956, S. Korea*

(Received January 19, 2012, Revised February 27, 2012, Accepted March 5, 2012)

Abstract. This study intends to explore dynamic interaction behaviors between actively controlled maglev vehicle and guideway girders by considering the nonlinear forms of electromagnetic force and current exactly. For this, governing equations for the maglev vehicle with ten degrees of freedom are derived by considering the nonlinear equation of electromagnetic force, surface irregularity, and the deflection of the guideway girder. Next, equations of motion of the guideway girder, based on the mode superposition method, are obtained by applying the UTM-01 control algorithm for electromagnetic suspension to make the maglev vehicle system stable. Finally, the numerical studies under various conditions are carried out to investigate the dynamic characteristics of the maglev system based on consideration of the linear and nonlinear electromagnetic forces. From numerical simulation, it is observed that the dynamic responses between nonlinear and linear analysis make little difference in the stable region. But unstable responses in nonlinear analysis under poor conditions can sometimes be obtained because the nominal air-gap is too small to control the maglev vehicle stably. However, it is demonstrated that this unstable phenomenon can be removed by making the nominal air-gap related to electromagnetic force larger. Consequently it is judged that the nonlinear analysis method considering the nonlinear equations of electromagnetic force and current can provide more realistic solutions than the linear analysis.

Keywords: maglev; guideway; dynamic interaction; electromagnetic suspension (ems); active control; surface irregularity

1. Introduction

Research on the maglev vehicle system has been prevalent since the 1970s because of the superior experience this system provides, such as through the provision of a comfortable ride, anti-noise feature, reduced risk of derailment, and a reduced cost for guideway girder maintenance. In particular, the test line for maglev was competitively constructed in Germany and Japan and as a result, maglev vehicle systems have been developed in many countries, including Korea. The first commercial maglev transportation, Transrapid, was operated in Shanghai, China. The UTM (urban transit maglev) system in Korea is currently being developed to provide effective transportation in

* Corresponding author, Professor, E-mail: kmye@skku.edu

metropolitan areas and it is expected to begin operating in 2012.

Most early research on the maglev system was performed on its simplified modeling, low vehicle speed, the linear electromagnetic force, and the active control algorithm. Cai *et al*. (1994) performed a parametric study on short-span bridges crossed by a 2-DOF (degree of freedom) maglev vehicle with passive spring and dashpot suspension. Tsunashima and Abe (1998) constructed a dynamic model for an active magnetic suspension and compared their results against field tests. Zheng *et al*. (2000) performed a numerical simulation of a coupled 5-DOF maglev vehicle and guideway system with a controllable feedback magnetic force. Meisinger (2002) performed the numerical simulation for a single-mass maglev vehicle on an elastic single- and double-span guideway moving with both constant magnet force and constant air-gap. Zhao and Zhai (2002) investigated the ride quality of a two-dimensional model of the German Transrapid maglev vehicle with an equivalent passive suspension running on a simple beam. Fang *et al*. (2004) studied the dynamic modeling and control of the Magplane vehicle. Morita *et al*. (2004) investigated the environmental influence on levitation control from the field test of the Linimo Line conducted during EXPO2005. Han *et al*. (2006) performed a finite element-based numerical simulation of the Korean UTM-01 maglev vehicle and guideway structures by using a large number of elements. Wang *et al*. (2007) performed the numerical dynamic simulation of the maglev vehicle and guideway system. Kwon *et al*. (2008) performed a numerical simulation for a 5-DOF maglev vehicle with equivalent passive suspension running on a suspension bridge under gusty winds in order to test the applicability of such a flexible bridge for the guideway structure. Concerning the vibration for maglev vehicles, Yau (2009, 2010a, b) performed a numerical simulation of the vibration and control of a maglev vehicle across diverse situations, such as wind and horizontal ground motion. Yaghoubi and Rezvani (2011) studied development of the maglev guideway loading model and Shibo *et al*. (2010) presented the coupled analysis results for the maglev vehicle and guideway system. Recently, some studies have begun to focus on nonlinear analyses considering the nonlinear characteristics of electromagnetic suspensions and the control algorithm. Hung (1991) developed a nonlinear controller of second- and third-order models for a magnetic levitation system and compared it against a traditional linear controller. Huang *et al.* (1999) then proposed a nonlinear adaptive back-stepping controller to stabilize the system under model uncertainty and achieve the desired servo performance in a 5-DOF system. Kaloust *et al.* (2004) presented a nonlinear robust control design for the levitation and propulsion of a magnetic levitation that guarantees global stability and robustness for a nonlinear 2-DOF maglev system. And Yang *et al.* (2011) investigated the robust control of a class of uncertain systems via a disturbance-observer-based control approach.

In this study, the dynamic nonlinear interaction behaviors between an actively controlled maglev vehicle and guideway girders are explored by considering the nonlinear equations of electromagnetic force and current exactly. For this purpose, dynamic equations of motion for a refined model of the maglev vehicle consisting of one car body, four bogies, and four electromagnet and two sensors per bogie are derived by considering electromagnetic forces, surface irregularity, and the deflection of the guideway girder. The equations of motion of the guideway girder based on the mode superposition method are then obtained by applying the UTM-01 control algorithm for electromagnetic suspension. Numerical studies under various conditions, such as those considering the deflection ratio of the guideway girder, roughness types, and increasing vehicle speed, are performed to investigate the dynamic characteristics of the maglev system from consideration of linear and nonlinear electromagnetic forces.

2. Dynamic equations of motion of a maglev vehicle and guideway girders

In this section, dynamic equations of motion for a refined model of the maglev vehicle and guideway girders are derived by considering nonlinear electromagnetic forces, surface irregularity, and the deflection of the guideway girder.

2.1 Electromagnetic force and current generated from an electromagnet

The electromagnetic force generated from the electromagnetic suspension shown in Fig. 1 can be derived by considering the force attraction between the electromagnetic and ferromagnetic objects. The electromagnetic force (Sinha 1987) acting on a track at any instant of time is expressed as

$$F_m(t) = \frac{\mu_0 N_m^2 A_m}{4}\left[\frac{i_0 + \Delta i(t)}{z_0 + \Delta z(t)}\right]^2 \tag{1}$$

where μ_0 = the magnetic permeability of vacuum; N_m and A_m = the number of turn of coil and effective areas of magnetic pole, respectively; i_0 and z_0 = initial current and nominal air-gap at static equilibrium; and $\Delta i(t)$ and $\Delta z(t)$ = fluctuations of current and air-gap while the maglev vehicle is running on the guideway.

The linearized electromagnetic force at the nominal equilibrium point can be then obtained as follows

$$F_m(t) = F_{m0} + k_i \Delta i(t) - k_z \Delta z(t) \tag{2}$$

and

$$k_i = \frac{\mu_0 N_m^2 A_m i_0}{2z_0^2},\quad k_z = \frac{\mu_0 N_m^2 A_m i_0^2}{2z_0^3},\quad F_{m0} = \frac{\mu_0 N_m^2 A_m i_0^2}{4z_0^2} \tag{3a,b,c}$$

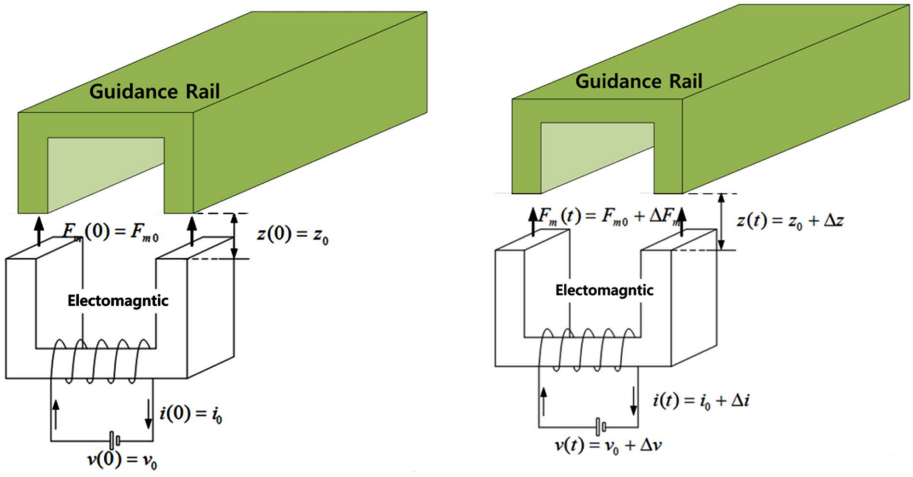

(a) $z(0) = z_0$ at equilibrium point (b) $z(t) = z_0 + \Delta z(t)$ during running time

Fig. 1 Electromagnetic suspension system

where k_i and k_z = the equivalent stiffnesses, which are dependent on the current and air-gap, respectively; and F_{m0} = the electromagnetic force at the nominal static equilibrium point.

On the other hand, Eq. (1) can be rewritten in the incremental form as follows

$$F_m = F_{m0} + k_i \Delta i(t) \frac{1 + \frac{\Delta i(t)}{2 i_0}}{\left(1 + \frac{\Delta z(t)}{z_0}\right)^2} - k_z \Delta z(t) \frac{1 + \frac{\Delta z(t)}{2 z_0}}{\left(1 + \frac{\Delta z(t)}{z_0}\right)^2} \tag{4}$$

Furthermore, the nonlinear relationship between the current rate, current, and voltage can be written as the following equation in terms of reluctance R and the inductance of magnet winding at equilibrium point L_0.

$$v_0 + \Delta v(t) = R\{i_0 + \Delta i(t)\} + \frac{\mu_0 N_m^2 A_m}{2} \frac{d}{dt}\left[\frac{i_0 + \Delta i(t)}{z_0 + \Delta z(t)}\right] \tag{5}$$

in which linearization of Eq. (5) leads to

$$\Delta \dot{i}(t) = \frac{k_z}{k_i} \Delta \dot{z}(t) - \frac{R}{L_0} \Delta i(t) + \frac{1}{L_0} \Delta v(t) \tag{6}$$

here

$$L_0 = \frac{\mu_0 N_m^2 A_m}{2 z_0} \tag{7}$$

Also, the incremental form of Eq. (5) can be exactly expressed as

$$\Delta \dot{i}(t) = \frac{k_z}{k_i}\left(\frac{1 + \Delta i(t)/i_0}{1 + \Delta z(t)/z_0}\right) \Delta \dot{z}(t) - \frac{R \Delta i(t)}{L_0}\left(1 + \frac{\Delta z(t)}{z_0}\right) + \frac{\Delta v(t)}{L_0}\left(1 + \frac{\Delta z(t)}{z_0}\right) \tag{8}$$

Considering four electromagnets and two sensors attached at each bogie, the following notations are adopted to compare the results with linear analysis with those easily obtained through nonlinear analysis.

$$B_{jk} = \frac{1 + \frac{\Delta i_{js}}{2 i_0}}{\left(1 + \frac{\Delta z_{jk}}{z_0}\right)^2}, \quad C_{jk} = \frac{1 + \frac{\Delta z_{jk}}{2 z_0}}{\left(1 + \frac{\Delta z_{jk}}{z_0}\right)^2}, \quad F_{js} = \frac{1 + \frac{\Delta i_{js}}{i_0}}{1 + \frac{\Delta z_{js}}{z_0}}, \quad E_{js} = 1 + \frac{\Delta z_{js}}{z_0} \tag{9a,b,c,d}$$

where Δi_{js} = the current at s^{th} sensor of j^{th} bogie; Δz_{jk} = the air-gap at k^{th} electromagnet of j^{th} bogie; Δz_{js} = the air-gap at s^{th} sensor of j^{th} bogie; and Δv_{js} = the voltage at s^{th} sensor of j^{th} bogie.

Now, note that Eqs. (9), (4) and (8) can be expressed as follows

$$F_{mjk} = F_{m0} + k_i \Delta i_{js} B_{jk} - k_z \Delta z_{jk} C_{jk} \tag{10}$$

$$\Delta \dot{i}_{js} = \frac{k_z}{k_i} F_{js} \Delta \dot{z}_{jk} - \frac{R}{L_0} E_{js} \Delta i_{js} + \frac{1}{L_0} E_{js} \Delta v_{js} \tag{11}$$

Here, it should be noted that the coefficients in Eq. (9) are equal to 1.0 in *linear* analysis so that Eqs. (10) and (11) are reduced to Eqs. (2) and (6), respectively. When equations of motion are

rigorously derived in the following sections, Δ is dropped for simplicity.

2.2 Nonlinear equations of motion for a maglev vehicle

Fig. 2 shows the idealized 10-DOF maglev vehicle consisting of one car body and four bogies. Four electromagnets and two sensors are attached at each bogie, which are connected with the car body through two secondary suspensions. From the dynamic force equilibrium of the free-body diagram in Fig. 3, the equations of motion for a car body subjected to the inertia force, spring, and damping forces of secondary suspensions and self-weight can be obtained as follows

$$m_c\ddot{z}_c = -\sum_{j=1}^{N_{bogi}}\sum_{i=1}^{2}[k_s z_{cbji} + c_s\dot{z}_{cbji}] \tag{12}$$

$$I_c\ddot{\theta}_c = \sum_{j=1}^{N_{bogi}}\sum_{i=1}^{2}(a_j + b_i)[k_s z_{cbji} + c_s\ddot{z}_{cbji}] \tag{13}$$

and

$$z_{cbji} = z_c - (a_j + b_i)\theta_c - z_{bj} + b_i\theta_{bj}, \quad \dot{z}_{cbji} = \dot{z}_c - (a_j + b_i)\dot{\theta}_c - \dot{z}_{bj} + b_i\dot{\theta}_{bj} \tag{14}$$

where m_c = mass of car body; I_c = mass moment of inertia about pitch motion of the car body; k_s and c_s = stiffness and damping of the secondary suspension; z_c = vertical displacement of the car body; a_j = distance from the car body center to j^{th} bogie; b_i = distance from the bogie center to i^{th} secondary suspension; θ_c = pitch angle of the car body; $\dot{z}_c$ = vertical velocity of the car body; $\dot{\theta}_c$ =

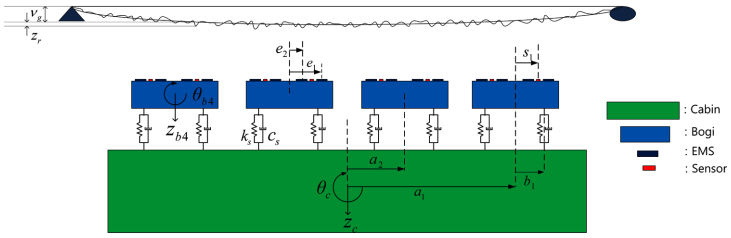

Fig. 2 Dynamic model for 10- DOF maglev vehicle and guideway girder

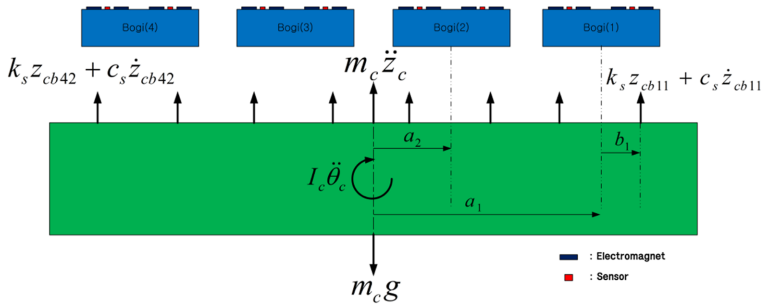

Fig. 3 Free-body diagram of the car body

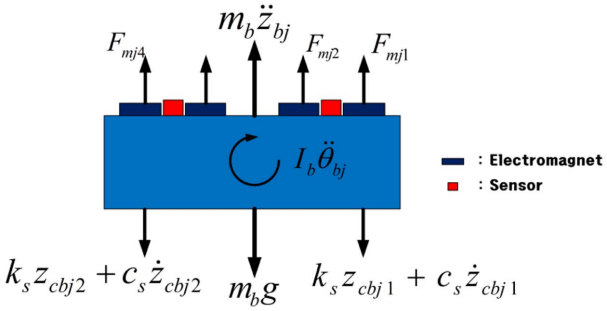

Fig. 4 Free-body diagram of the j^{th} bogie

pitch angular velocity of the car body; $\ddot{z}_c$ = vertical acceleration of the car body; and $\ddot{\theta}_c$ = pitch angular acceleration of the car body.

Similarly, by considering inertia forces and the self-weights of bogies, the spring and damping forces of secondary suspensions, and the electromagnetic forces between electromagnetic suspension and the guideway girder (see Fig. 4), equations of motion for each bogie are obtained as

$$m_b\ddot{z}_{bj} = \sum_{i=1}^{2}[k_s z_{cbji} + c_s \dot{z}_{cbji}] + \sum_{k=1}^{N_{ems}} F_{mjk} \qquad j = 1, 2, 3, 4 \tag{15}$$

$$I_{bj}\ddot{\theta}_{bj} = -\sum_{i=1}^{2} b_i[k_s z_{cbji} + c_s \dot{z}_{cbji}] + \sum_{k=1}^{N_{ems}} e_k F_{mjk} \qquad j = 1, 2, 3, 4 \tag{16}$$

where F_{mjk} is the magnetic force at k^{th} electromagnet of j^{th} bogie and referring to Eq. (10), it is expressed as

$$F_{mjk} = F_{m0} + k_i i_{js} B_{jk} - k_z C_{jk}(z_{bj} - e_k \theta_{bj} - v_{gjk} - z_{rjk}) \tag{17}$$

where m_b = mass of each bogie; I_b = mass moments of inertia about pitch motion of bogie; z_{bj} = vertical displacement of j^{th} bogie; θ_{bj} = pitch angle of j^{th} bogie; $\dot{z}_{bj}$ = vertical velocity of j^{th} bogie; $\dot{\theta}_{bj}$ = pitch angular velocity of j^{th} bogie; $\ddot{z}_{bj}$ = vertical acceleration of j^{th} bogie; $\ddot{\theta}_{bj}$ = pitch angular acceleration of j^{th} bogie; i_{jk} = current at k^{th} electromagnet of j^{th} bogie; e_k = distance from bogie center to k^{th} electromagnet; v_{gjk} = vertical displacement of guideway girder at k^{th} electromagnet of j^{th} bogie; z_{jk} = air-gap at k^{th} electromagnet of j^{th} bogie; and z_{rjk} = surface roughness of guideway at k^{th} electromagnet of j^{th} bogie given in section 2.5.

In the case of a linear system, Eq. (17) is replaced by

$$F_{mjk} = F_{m0} + k_i i_{js} - k_z(z_{bj} - e_k \theta_{bj} - v_{gjk} - z_{rjk}) \tag{18}$$

2.3 Equations of motion for guideway structures based on the mode superposition method

Because the number of degrees of freedom of the stiffening girder is generally much larger than that of the maglev vehicle, reducing the number of equations by applying the mode superposition method to the stiffening girder appears reasonable for computational efficiency. The mode superposition

method is a very powerful method used to reduce the number of unknowns in a dynamic response analysis. By applying the expansion theorem, the vertical displacements of the stiffening girder at kth electromagnet of j^{th} bogie can be expressed as a summation of each component of the normalized mode shape $\varnothing_n(x)$ and generalized coordinate $q_n(t)$

$$v_{gjk} = \sum_{n=1}^{N_{mode}} \varnothing_n(x_{jk}) q_n(t) \tag{19}$$

Now, noting that the guideway girder is subjected to magnetic forces generated from each electromagnetic suspension, coupled equations of motion for girders based on the mode superposition method can be obtained as

$$\ddot{q}_n(t) + 2\xi_n \omega_n \dot{q}_n(t) + \omega_n^2 q_n(t) = \sum_{i=1}^{N_{bogi}} \sum_{k=1}^{N_{ems}} \varnothing_n(x_{jk}) \{F_{m0} + k_i i_{jk} B_{jk} - k_z C_{jk}(z_{bj} - e_k \theta_{bj} - v_{gjk} - z_{rjk})\} \tag{20}$$

where $\omega_n = n^{th}$ mode natural frequency of guideway; and $\xi_n = n^{th}$ mode damping ratio of guideway.

2.4 Active control algorithm applied to a maglev vehicle

The active control system is an essential part of the maglev vehicle running on the guideway because the operation of the maglev system cannot be stably supported by the static electromagnetic force. To keep the running maglev train stable, it is important to select an appropriate control algorithm among the several modern control methods, which is dependent on the objective of control, availability of measurements for feedback, and the nature of external disturbances. In particular, since it is impossible and unnecessary to measure all state variables, some selected output variables that depend on the state variables need to be measured in practice, which means that an observer is inevitably required for state estimation.

In this study, the UTM01 controller which is used in the test maglev line in Korea is applied for actively controlling electromagnetic suspension in which vertical acceleration $\ddot{z}_{bjs}$ and air-gap g_{js} are measured at sensors attached to bogies (see Fig. 2). The detailed control algorithm can be expressed as follows (Han *et al*. 2008)

$$\dot{\hat{x}}_s = A_x \hat{x}_s + L_s y_s \tag{21}$$

where

$$\hat{x}_s = \{\hat{x}_{1js}, \hat{x}_{2js}, \hat{x}_{3js}, \hat{x}_{4js}, \hat{x}_{5js}\}^T, \quad y_s = \{\ddot{z}_{bjs}, g_{js}\}^T \tag{22a,b}$$

$$A_s = \begin{bmatrix} 0 & \frac{1}{T_3} & 0 & \frac{-1}{T_3} & 0 \\ \frac{-1}{T_1} & \frac{-V_1}{T_3} & 0 & \frac{V_1}{T_1} & 0 \\ 0 & \frac{1}{T_2} & \frac{-V_2}{T_2} & 0 & \frac{V_2}{T_2} \\ 0 & 0 & 0 & \frac{-V_3}{T_4} & \frac{-1}{T_4} \\ 0 & 0 & 0 & \frac{1}{T_5} & 0 \end{bmatrix}, \qquad L_s = \begin{bmatrix} 0 & 0 \\ \frac{1}{T_1} & 0 \\ 0 & 0 \\ 0 & \frac{1}{T_4} \\ 0 & 0 \end{bmatrix} \tag{23a,b}$$

Table 1. Properties of the UTM-01 control parameter

Index	Specification	Index	Specification
k_1	33	T_3	0.3439
k_2	495	T_4	0.000242
k_3	0	T_5	0.022
k_4	26400	V_1	1.43
k_5	49500	V_2	1.1
T_1	0.22	V_3	0.22
T_2	0.011		

where $\hat{x}_{js}$ = the estimated state vector at s^{th} senor of j^{th} bogie; $\ddot{z}_{bjs}$ = the observed vertical acceleration at s^{th} senor of j^{th} bogie; g_{js} = the observed air-gap between bogie and guideway; s_s = the distance from center of bogies to s^{th} sensor; v_{gjs} = the displacement of girder at s^{th} sensor of j^{th} bogie; and z_{rjs} = the surface roughness of guideway at s^{th} sensor of j^{th} bogie.

In Eq. (22(b)), the observed acceleration and the observed air-gap are expressed with respect to state variables as

$$\ddot{z}_{bjs} = \ddot{z}_{bj} - s_s \ddot{\theta}_{bj}, \qquad g_{js} = z_{bj} - s_s \theta_{bj} - v_{gjs} - z_{rjs} \tag{24}$$

where

$$v_{gjs} = \sum_{n=1}^{N_{mode}} \varnothing_n(x_{js}) q_n(t) \tag{25}$$

Now, the voltages at each electromagnet are determined from the estimated state vector and the acceleration measured at the connected sensor as follows

$$v_{js} = k_1 \ddot{z}_{bjs} - k_1 \hat{x}_{1js} + (-k_1 V_1 + k_2)\hat{x}_{2js} + k_3 \hat{x}_{3js} + (k_1 V_1 + k_4)\hat{x}_{4js} + k_5 \hat{x}_{5js} \tag{26}$$

where v_{js} = the voltage at s^{th} sensor of j^{th} bogie. The coefficients used in Eqs. (23) and (24) are given in Table 1.

2.5 Surface irregularity of the guideway

Instead of applying artificial surface irregularity generated from the power spectral density (PSD) function, the actual roughness of the maglev guideway is used to evaluate practical dynamic responses in this study. Fig. 5 shows the irregularity profiles of guideway surface that were measured at the test tract in the Korean Institute of Machinery and Materials (KIMM). The roughness profiles, which have a maximum irregularity ranging around −3.704 mm ~ 4.124 mm, were measured at every 1.25 m along the test tract. Three types of roughness are used to simulate dynamic responses under the various conditions. The first type is a normal condition based on the measured profile data, which has a maximum irregularity ranging around −3.704 mm ~ 4.124 mm. The second and third types are fair and poor conditions, respectively, with maximums of −1.852 mm ~ 2.062 mm and −5.550 mm ~ 6.186 mm, respectively. The fair and poor conditions are only given for comparative studies by changing the amplitude scales 0.5 and 1.5 of the normal condition.

Table 2. Maximum irregularity range of roughness

Index	Condition	Range of roughness (mm)
KIMM01	Fair	−1.852 ~ 2.062
KIMM02	Normal	−3.704 ~ 4.124
KIMM03	Poor	−5.550 ~ 6.186

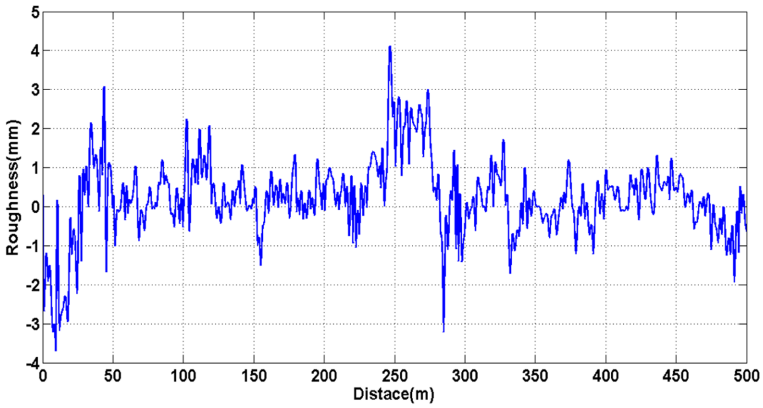

Fig. 5 Vertical roughness of the test tract at KIMM

2.6 Coupled dynamic equations of motion for the vehicle, guideway girder, and control system

A maglev train consisting of 1 car body and 4 bogies has 10 degrees of freedom, 8 current variables, and 40 estimated state variables for the active control system because 2 sensors and 4 electromagnets are attached at each bogie. A girder also has n-tuple mode variables. As a result, the maglev-guideway coupled system has 78 state-space variables that consist of 20 variables for a maglev vehicle, two times the 5-tuple mode variables per guideway girder, 8 variables for current, and 40 variables for electromagnets. In addition, if a maglev vehicle is running over two girders through hinged supports, the state-space variables for girders can double.

Now, by combining Eqs. (12) and (13) for a car body, Eqs. (15) and (16) for bogies, Eq. (20) for the guideway, Eq. (11) for currents, and Eq. (21) for the estimator, the total state-space equation can be written as follows

$$\dot{x}(t) = A(t)x(t) + f(t) \tag{27}$$

where

$$x = \{x_b;\ x_v;\ \hat{x}\}^T, \quad A = \begin{bmatrix} A_{bb} & A_{bv} & A_{b\hat{x}} \\ A_{vb} & A_{vv} & A_{v\hat{x}} \\ A_{\hat{x}b} & A_{\hat{x}v} & A_{\hat{x}\hat{x}} \end{bmatrix} \tag{28a,b}$$

$$x_b = \{q_1, \ldots, q_{nmode}, \dot{q}_1, \ldots, \dot{q}_{nmode}\}^T$$

$$x_v = \{z_c, \dot{z}_c, z_{bi}, \dot{z}_{b1}, \theta_{b1}, \dot{\theta}_{b1}, \ldots, \theta_{b4}, \dot{\theta}_{b4}, i_{11}, i_{12}, \ldots, i_{41}, i_{42}\}^T \tag{29a,b}$$

$$\hat{x} = \{\hat{x}_{111}, \hat{x}_{21}, \hat{x}_{311}, \hat{x}_{411}, \hat{x}_{511}, \ldots, \hat{x}_{442}, \hat{x}_{542}\}^T$$

Clearly, Eq. (27) represents a time-varying nonlinear system based on Eq. (10) for a nonlinear magnetic force. The MATHEMATICA commercial scientific software was used to derive the mathematical expressions for sub-matrices of $A(t)$, $f(t)$ and the detailed expression of $A(t)$, $f(t)$ for a maglev vehicle having 1 car body, 1 bogie, 1 electromagnet, and 1 sensor per bogie, as presented in the Appendix. Finally, the above simultaneous ordinary differential equation may be solved with the 4th Runge-Kutta method (Nakamura 2002)

$$x_{i+1} = x_i + \frac{\Delta t}{6}(k_1 + k_2 + k_3 + k_4) \tag{30}$$

where

$$k_1 = A(t_i)x_i + f(t_i) \tag{31a,b,c,d}$$

$$k_2 = A\left(t_i + \frac{\Delta t}{2}\right)\left(x_i + k_1\frac{\Delta t}{2}\right) + f\left(t_i + \frac{\Delta t}{2}\right)$$

$$k_3 = A\left(t_i + \frac{\Delta t}{2}\right)\left(x_i + k_2\frac{\Delta t}{2}\right) + f\left(t_i + \frac{\Delta t}{2}\right)$$

$$k_4 = A(t_i + \Delta t)(x_i + k_3\Delta t) + f(t_i + \Delta t)$$

3. Numerical simulation

Some numerical examples of for the dynamic interaction responses of the maglev vehicle and guideway structure are given here in order to investigate the effects of nonlinear magnetic forces on the coupling response. The vehicle used in this study is the maglev model, which is very similar to the UTM-01 model. Basically, the maglev in operation is assumed to consist of only one car. The translational speed of each car body and bogies are supposed to be constant and the basic properties of maglev vehicle are given in Table 3.

The simple guideway girder shown in Fig. 6(a), which was proposed by Jin *et al* (2007), is used to investigate the dynamic responses of the guideway system analytically in this study. The span length of each girder is basically 25 m. By adjusting the height of the box girder, the ratio between one span length and maximum static deflection ranges from 500 to 4000 for the parametric study. The geometric properties for guideway girders are given in Table 4.

Parametric studies are carried out under a variety of parameters, such as those including the deflection ratio, vehicle speed, roughness types, and initial conditions for the nominal air-gap. As a result, the dynamic responses of the maglev vehicle and the girder, such as through the air-gap, the acceleration of the car body, bridge deflection, current, the acceleration of the bogie, and voltage, are presented and compared for the linear and nonlinear system.

3.1 Comparison of numerical analysis results of linear and nonlinear magnetic forces

To compare numerical results with dynamic interaction analysis, considering both linear and nonlinear magnetic forces, linear and nonlinear analyses are performed under the following condition:

- Vehicle Speed: 300 km/h

Table 3. Material properties of the maglev model

Index		Value
Mass of car body (m_c)	Full	19000 kg
Mass moment of inertia of car body	I_c	1419000 kg·m²
Mass of bogie	m_b	1015 kg
Mass moment of inertia of bogie	I_b	557.8 kg·m²
Spring constant and damping coefficient of air spring	k_s	8×10^4 N/m
	c_s	5.2×10^4 N·s/m
Electromagnet	μ_0	$4\pi \times 10^{-7}$
	N	400 turn
	A	0.036 m²
	i_0	15.56 A
	z_0	8 mm
	R	0.6 Ω

(a) Guideway girder (b) Cross section of the guideway girder

Fig. 6 The guideway girder with the box-typed cross section

Table 4. Geometric properties of the guideway girder

Deflection ratio	Maximum displacement (mm)	Width (m)	Height (m)	Thickness (m)	A(m^2)	Area moment of inertia(m^4)	Mass per unit length(ton m^{-1})	First natural frequency(Hz)
500	50.0	1.35	0.93	0.2	0.75	0.078	2.25	2.56
1000	25.0	1.35	1.21	0.2	0.86	0.157	2.59	3.38
1500	16.7	1.35	1.41	0.2	0.95	0.235	2.84	3.95
2000	12.5	1.35	1.58	0.2	1.01	0.314	3.04	4.41
2500	10.0	1.35	1.72	0.2	1.70	0.392	3.21	4.80
3000	8.3	1.35	1.85	0.2	1.12	0.471	3.36	5.13
3500	7.14	1.35	1.96	0.2	1.67	0.550	3.50	5.61
4000	6.25	1.35	2.07	0.2	1.21	0.628	3.62	5.90

- Roughness: KIMM02
- Time interval: 0.001 sec
- Deflection ratio: 3000

Fig. 7 shows the time history responses over the running distance of 750 m for the vehicle speed of

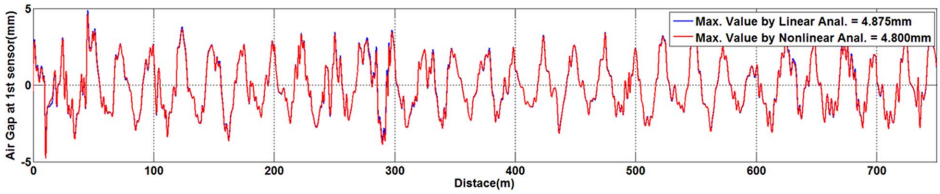

(a) Air-gap fluctuation at the first sensor of the first bogie

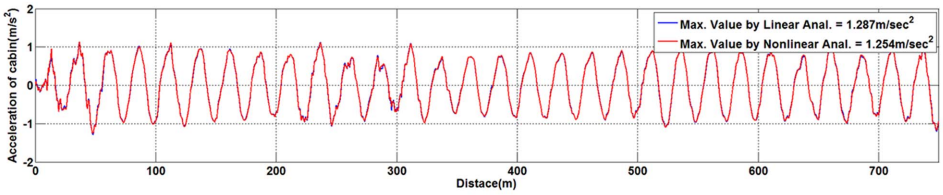

(b) Vertical acceleration at the center of the car body

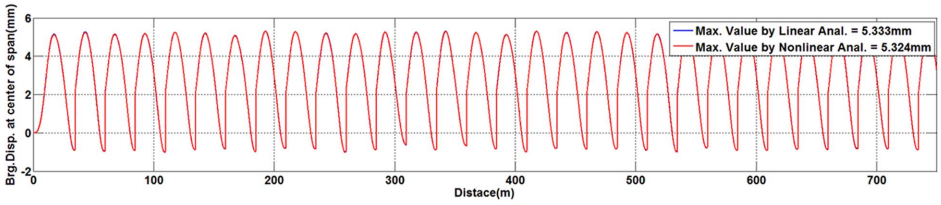

(c) Vertical displacement at the center of the guideway girder

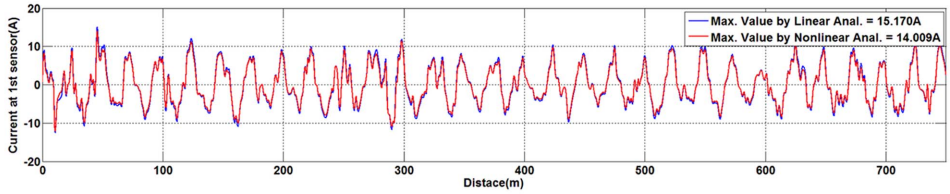

(d) Current at the first sensor of the first bogie

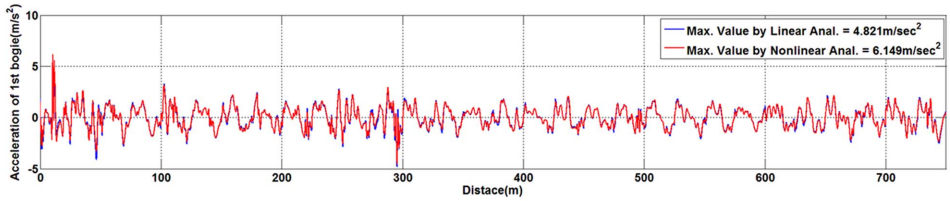

(e) Vertical acceleration at the center of the first bogie

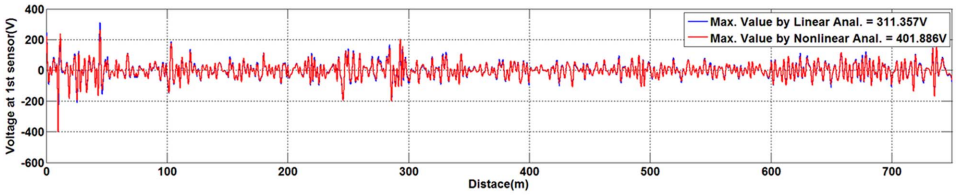

(h) Voltage at the first sensor of the first bogie

Fig. 7 Time history responses by linear and nonlinear analysis
(vehicle speed = 300 km/h, roughness type = KIMM02, and deflection ratio = 3000)

300 km/h and the deflection ratio of 3000 by nonlinear and linear analysis, respectively. From Fig. 7, it is clear that the time history responses between nonlinear and linear analysis make little difference along the simulated distance. In the strict sense, however, maximum values of responses by nonlinear analysis are slightly lower from those achieved by linear analysis, except for the voltage. It is also observed in Fig. 7(h) that the maximum value of the voltage in nonlinear analysis has been increased 1.33 times more than that in linear analysis at the distance of 10 m, which corresponds to the minimum air-gap locally in Fig. 7(a).

It is considered that the responses can be amplified due to the nonlinear terms in Eq. (9) if the air-gap between the guideway girder and the bogie is smaller. Thus, to explore this phenomenon in detail, the following analysis is carried out under the poor roughness condition:

- Vehicle Speed: 300 km/h
- Roughness: KIMM03
- Time interval: 0.001 sec
- Deflection ratio: 3000

Fig. 8 shows that the maglev system remains stable in linear analysis, but the system diverges unstably around 10 m distance in nonlinear analysis. This phenomenon can be explained based on the nonlinear expression (10) for the magnetic force generated from the electromagnet. That is, as the air-gap z_{bgjk} in Fig. 8(a) approaches −6.5 mm around 10 m distance, the denominator $\{1 + (z_{bgjk}/z_0)\}^2$ of B_{jk}, C_{jk} in Eq. (9) become so small with the nominal air-gap z_0 of 8 mm. As a result, the factors B_{jk}, C_{jk} become so large that the voltage can fluctuate unstably, as can be seen in Fig. 8(h). This means that the analysis considering the nonlinear magnetic force can provide more realistic solutions than the linear analysis.

To investigate dynamic characteristics between the responses as the vehicle speed is increased to 700 km/h, parametric studies are carried out under the following condition:

- Vehicle Speed: 50~700 km/h
- Roughness: KIMM02
- Time interval: 0.001 sec
- Deflection ratio: 2000, 3000

Fig. 9 shows the maximum and RMS values of the dynamic response, such as the air-gap, acceleration of the car body, current, and voltage by linear and nonlinear analysis with the defection ratios of 2000 and 3000. It is found in Fig. 9 that the difference in the results offered by the two types of analysis is not significant in the stable range, but maximum responses for the defection ratios of 3000 are overall smaller than those for the defection ratios of 2000. Significantly, when the speed of the maglev vehicle running on the guideway girder with the deflection ratio of 2000 exceeds 300 km/h, the numerical result from nonlinear analysis shows that the system can diverge unstably.

3.2 Effect of nominal air-gap in nonlinear analysis

As shown in Eq. (3(c)), the nominal air-gap z_0, which has a great influence on the driving stability of the maglev system, and the initial current i_0 are directly related to the nominal magnetic force F_{m0}. Here, F_{m0} is a given value which is determined from the equilibrium condition with the weight of maglev vehicle and i_0 can be evaluated dependent on the variation of z_0. To investigate the effects of the nominal air-gap on the dynamic responses, nonlinear interaction analyses are performed under the following conditions:

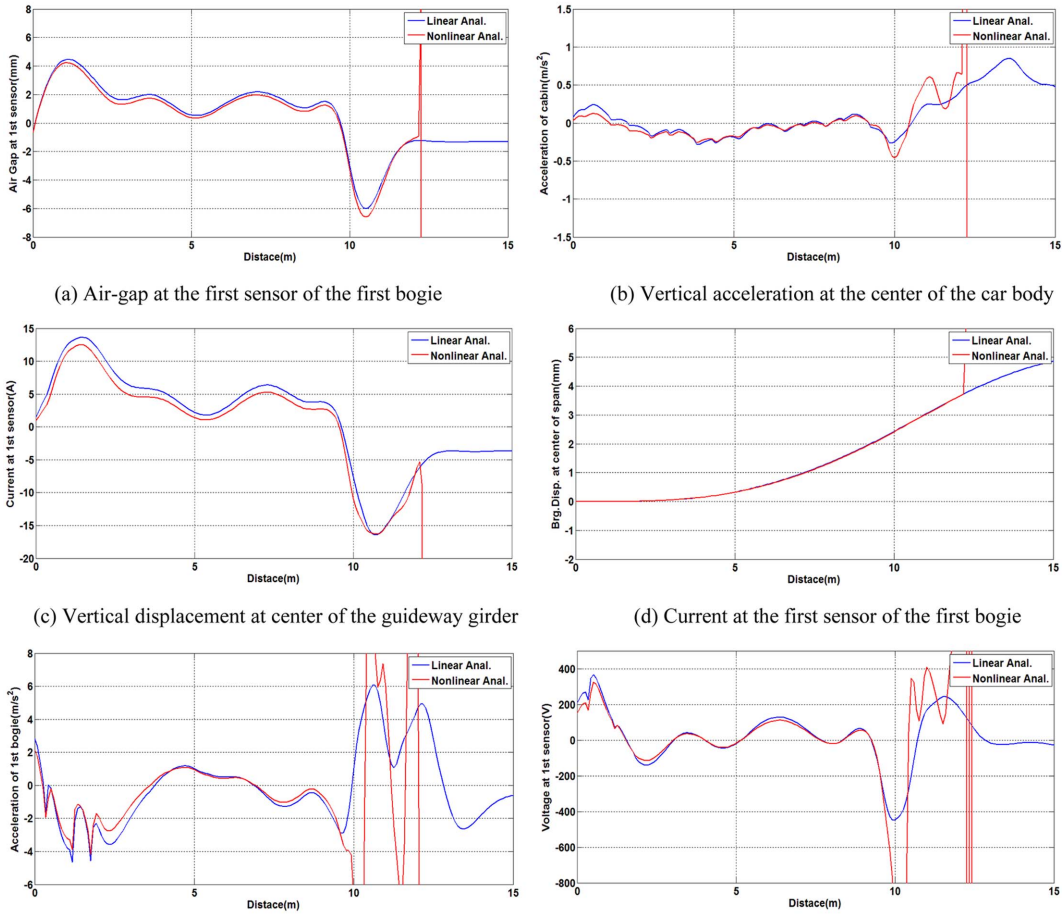

(a) Air-gap at the first sensor of the first bogie

(b) Vertical acceleration at the center of the car body

(c) Vertical displacement at center of the guideway girder

(d) Current at the first sensor of the first bogie

(e) Vertical acceleration at the center of the first bogie

(h) Voltage at the first sensor of the first bogie

Fig. 8 Time history responses by linear and nonlinear analysis
(vehicle speed = 300 km/h, roughness type = KIMM03, and deflection ratio = 3000)

- Vehicle Speed: 50 ~ 700 km/h
- Roughness: KIMM02
- Time interval: 0.001 sec
- Deflection ratio: 2000
- $z_0 = 10\ mm$, $i_0 = 19.45\ A$; $z_0 = 12\ mm$, $i_0 = 23.33\ A$; $z_0 = 16\ mm$, $i_0 = 31.11\ A$

Fig. 10 shows the DAF (dynamic amplification factor) of the vertical deflection and bending moment at the center of the guideway girder through an increase to the vehicle's speed, respectively, where DAF is defined as the ratio between maximum values obtained from dynamic and static analysis as a maglev vehicle moves on the guideway structure. From Fig. 10, it can be noted that DAFs steadily increase in proportion to the vehicle speed. In addition, it is observed that the DAF for the deflection is almost the same as that for the bending moment at the low and medium speed, but the deflection's DAF is higher at the high speed. Furthermore, the DAF tends to be much smaller at a low speed, but to be large as the vehicle speed is increased. Thus, it is concluded that the DAF of the maglev train is dominated by high vehicle speed. In addition, it is observed that

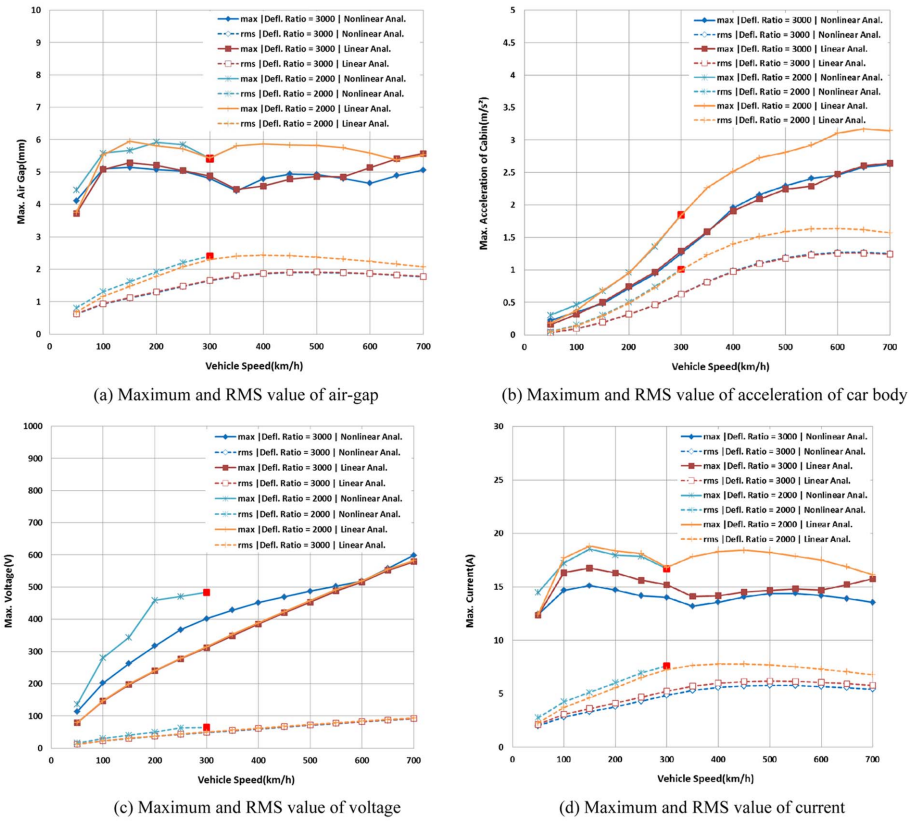

(a) Maximum and RMS value of air-gap

(b) Maximum and RMS value of acceleration of car body

(c) Maximum and RMS value of voltage

(d) Maximum and RMS value of current

Fig. 9 Effect of vehicle speed on dynamic responses from linear and nonlinear analysis (Roughness type = KIMM02, vehicle Speed = 50 ~ 700 km/h, and deflection ratio = 2000, 3000)

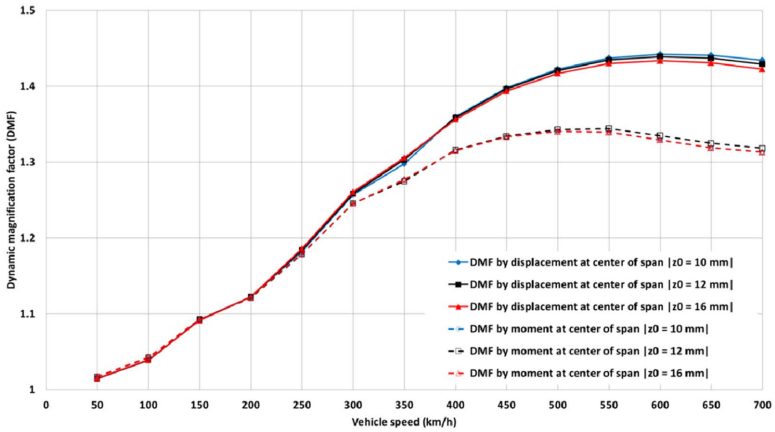

Fig. 10 Dynamic amplification factor (DAF) of guideway structures by displacement and moment at center of span (Roughness type = KIMM02, damping ratio of guideway structure, = 0.02, deflection ratio = 2000)

DAF is not sensitive to the fluctuation of z_0.

On the other hand, Fig. 11 shows variations in the maximum values and RMS responses by

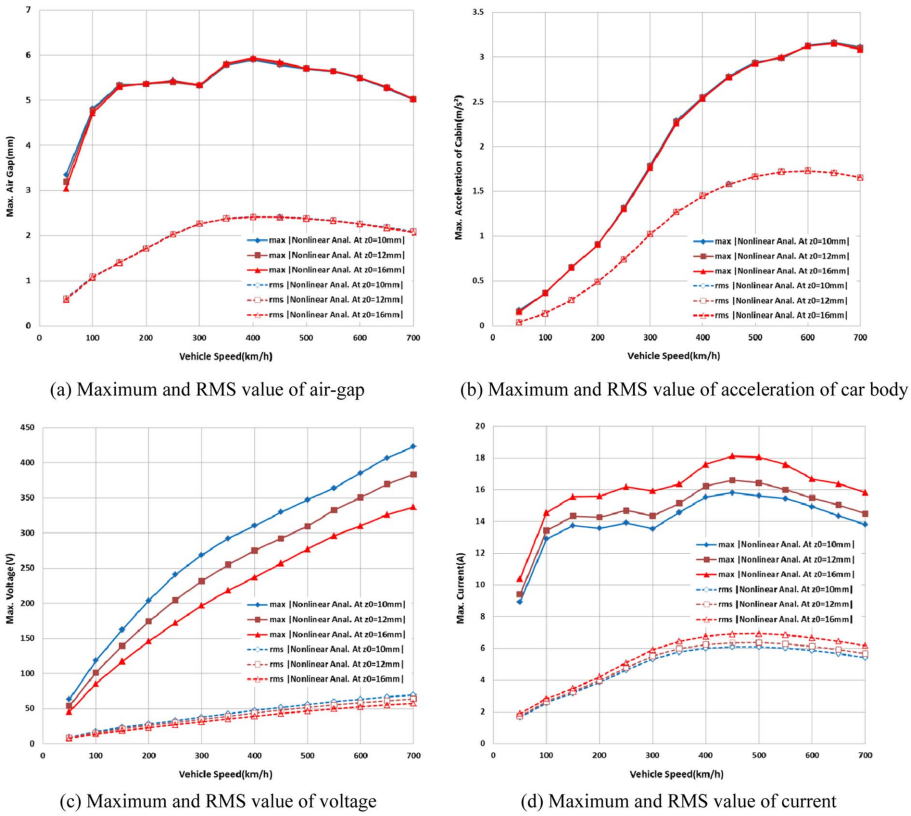

(a) Maximum and RMS value of air-gap

(b) Maximum and RMS value of acceleration of car body

(c) Maximum and RMS value of voltage

(d) Maximum and RMS value of current

Fig. 11 Effect of initial air-gap and current in nonlinear analysis at z
(Roughness type = KIMM02, vehicle Speed = 50 ~ 700 km/h, and deflection ratio = 2000)

nonlinear analysis with the nominal air-gap increasing as the vehicle speed is increased. From Fig. 11, it is observed that the maximum value and RMS of the air-gap and the acceleration of the car body are not much different with the variation of the nominal air-gap. Contrary to this finding, the maximum values of the voltage at the electromagnet become smaller when the nominal air-gap increases and those of the current become inversely larger when the nominal air-gap increases.

4. Conclusions

The purpose of this study is to examine the dynamic interaction responses between an actively controlled maglev vehicle and guideway girders by applying the nonlinear equation for electromagnetic force and current. The maglev model for the proposed ten degree of freedom maglev vehicle consists of one car body and four bogies, and each bogie is comprised of four electromagnets and two sensors and connected with the car body through two secondary suspensions. The displacements of the stiffening girder are expressed by the mode superposition method, and the UTM-01 control algorithm for electromagnetic suspension is applied to make the maglev vehicle system stable. The state-space equation is finally obtained by combining equations of the maglev vehicle, guideway girders, and active control system. Various dynamic responses, such as those

including the air-gap, the acceleration of the car body, bridge deflection, current, the acceleration of the bogie, and voltage by the linear and nonlinear system, are investigated under diverse conditions, such as those including the deflection ratio, increasing vehicle speed, various roughness types, and initial conditions. From the parametric study, the following conclusions can be drawn:

1. The overall dynamic responses to nonlinear and linear analysis make little difference under good conditions, such as at low vehicle speed, under the good roughness condition, the large deflection ratio, and the large nominal air-gap.
2. From the numerical results obtained by linear and nonlinear analysis, it is observed that the responses can be greatly amplified due to the nonlinear magnetic force when the total air-gap is so small that the bogie is very close to the guideway girder.
3. Furthermore, the maglev system under bad conditions can sometimes diverge unstably in nonlinear analysis, but the maglev vehicle remains stable in linear analysis.
4. Accordingly, to cure this problem radically, the nominal air-gap in the static state needs to be enlarged by making the car body lighter or increasing the initial current.
5. Finally, the DAF of the maglev train is greatly dominated by high vehicle speed and the DAF for deflection is almost the same as that for the bending moment at the low and medium speed, but the deflection's DAF is higher at the super-high speed.

References

Cai, Y., Chen, S.S., Rote, S.M. and Coffey, H.T. (1994), "Vehicle/guideway interaction for high speed vehicles on a flexible guide-way", *J. Sound Vib*., **175**(5), 625-646.

Fang, J., Ardovinsky, A. and Montgomery, D.B. (2004), "Dynamic modeling and control of the Magplane vehicle", *Proceedings of the 18th International Conference on Magnetically Levitated Systems and Linear Drives (Maglev' 2004)*, Shanghai, China.

Yaghoubi, H. and Rezvani, M.A. (2011), "Development of maglev guideway loading model, *J. Transp.Eng.-ASCE*, **137**(3), 201-213.

Han, S.H., Kim, Y.J., Shin, B.C. and Kim, B.H. (2006), "Simulation of dynamic interaction between maglev and guideway using FEM", *Proceedings of the 19th International Conference on Magnetically Levitated Systems and Linear Drives (Maglev' 2006)*, Dresden, Germany.

Han, H.S., Kim, S., Yim, B. and Hur, Y. (2008), "Stability analysis of a Maglev vehicle utilizing electromagnetic suspension system", *Trans.Korean Soc. Auto. Eng*., **16**(3), 118-126.

Huang, C.M., Chen, M.S. and Yen, J.Y. (1999), "Adaptive nonlinear control of repulsive Maglev suspension systems", *Proceedings of the International Conference on Control Applications(IEEE'1999)*, Hawaii, USA.

Hung, J.Y. (1991), "Nonlinear control of a magnetic levitation system", *Proceedings of the Industrial Electronics, Control and Instrumentation (IECON '91)*, Kobe, Japan.

Jin, B.M., Kim, I.G., Kim ,Y.J., Yeo, I.H., Chung, W.S. and Moon, J.S. (2007), "Proposal of maglev guideway girder by structural optimization : civil works of center for urban maglev program in Korea", *Proceedings of the International Conference on Electrical Machines and Systems*, Seoul, Korea.

Kaloust, J., Ham, C., Siehling, J., Jongekryg, E. and Han, Q. (2004), "Nonlinear robust control design for levitation and propulsion of a maglev system", *Proceedings of the IEE Proceedings Control Theory & Applications*, **151**(4), 460-464.

Kwon, S.D., Lee, J.S., Moon, J.W. and Kim, M.Y. (2008), "Dynamic interaction analysis of urban maglev vehicle and guideway suspension bridge subjected to gusty wind", *Eng. Struct*., **30**(12), 3445-3456.

Lee, J.S., Kwon, S.D., Kim, M.Y. and Yeo, I.H. (2009), "A parametric study on the dynamics of urban transit maglev vehicle running on flexible guideway bridges", *J. Sound Vib*., **328**(3), 301-317.

Meisinger, R. (2002), "Simulation of a single and double-span guideway under action of moving maglev vehicles with constant force and constant gap", *Proceedings of the* Schriftenreihe der Georg-Simon-Ohm Fachhochschule

Nu¨rnberg Nr.14, Nurnberg, Germany.
Morita, M., Iwaya, M. and Fujino, M. (2004), "The characteristics of the levitation system of Linimo (HSST system)", *Proceedings of the 18th International Conference on Magnetically Levitated Systems and Linear Drives (Maglev'2004)*, Shanghai, China.
Nakamura, S. (2002), *Numerical analysis and graphic visualization with MATLAB*, Prentice Hall.
Shibo, Ren, Arie, Romeijn and Kees Klap (2010), "Dynamic simulation of the maglev vehicle/guideway system, *J. Bridge Eng*., **15**(3).
Sinha, P.K. (1987), *Electromagnetic suspension-dynamics and control*, IEE.
Tsunashima, H. and Abe, M. (1998), "Static and dynamic performance of permanent magnet suspension for maglev transport vehicle", *Vehicle Syst. Dyn*., **29**(2), 83-111.
Wang, H.P., Li, J. and Zhang, K. (2007), "Vibration analysis of the maglev guideway with the moving load", *J. Sound Vib*., **305**(4-5), 621-640.
Yang, J., Zoltas, A., Chen, W.H., Michail, K. and Li, S. (2011), "Robust control of nonlinear MAGLEV suspension system with mismatched uncertainties via DOBC approach", *ISAT*., **50**(3), 389-396.
Yau, J.D. (2009), "Vibration control of maglev vehicles traveling over a flexible guideway", *J. Sound Vib*., **321**(1-2), 184-200.
Yau, J.D. (2010a), "Interaction response of maglev masses moving on a suspended beam shaken by horizontal ground motion", *J. Sound Vib*., **329**(2), 171-188.
Yau, J.D. (2010b), "Aerodynamic vibrations of a maglev vehicle running on flexible guideways under oncoming wind actions", *J. Sound Vib*., **329**(1), 1743-1759.
Zhao, D.F. and Zhai, W.M. (2002), "Maglev vehicle/guideway vertical random response and ride quality, *Vehicle Syst. Dyn.*, **38**(3), 185-210.
Zheng, X.J., Wu, J. J. and Zhou, Y.H. (2000), "Numerical analysis on dynamic control of five-degree-of-freedom maglev vehicle moving on flexible guideways", *J. Sound Vib*., **235**(1), 43-61.

Appendix. The sub-matrices in Eq. (27) for 1-car body, 1-bogie, 1-electromagnet and 1-sensor

$$\dot{\boldsymbol{x}} = \boldsymbol{A}\boldsymbol{x} + \boldsymbol{F}$$

$$\dot{\boldsymbol{x}} = \begin{Bmatrix} \dot{q}_1 \\ \dot{q}_2 \\ \vdots \\ \dot{q}_n \\ \ddot{q}_1 \\ \ddot{q}_2 \\ \vdots \\ \ddot{q}_n \\ \dot{z}_c \\ \dot{z}_b \\ \ddot{z}_c \\ \ddot{z}_b \\ \dot{i} \\ \dot{\hat{x}}_{111} \\ \dot{\hat{x}}_{211} \\ \dot{\hat{x}}_{311} \\ \dot{\hat{x}}_{411} \\ \dot{\hat{x}}_{511} \end{Bmatrix}_{(2n+10)\times 1} \quad \boldsymbol{x} = \begin{Bmatrix} q_1 \\ q_2 \\ \vdots \\ q_n \\ q_1 \\ q_2 \\ \vdots \\ q_n \\ z_c \\ z_b \\ \dot{z}_c \\ \dot{z}_b \\ i \\ \hat{x}_{111} \\ \hat{x}_{211} \\ \hat{x}_{311} \\ \hat{x}_{411} \\ \hat{x}_{511} \end{Bmatrix}_{(2n+10)\times 1} \quad \boldsymbol{A} = \begin{bmatrix} \boldsymbol{0}_{n\times n} & \boldsymbol{I}_{n\times n} & \boldsymbol{0}_{n\times 2} & \boldsymbol{0}_{n\times 2} & \boldsymbol{0}_{n\times 1} & \boldsymbol{0}_{n\times 5} \\ \boldsymbol{A}_{21} & \boldsymbol{A}_{22} & \boldsymbol{A}_{23} & \boldsymbol{0}_{n\times 2} & \boldsymbol{A}_{25} & \boldsymbol{0}_{n\times 5} \\ \boldsymbol{0}_{2\times n} & \boldsymbol{0}_{2\times n} & \boldsymbol{0}_{2\times 2} & \boldsymbol{I}_{2\times 2} & \boldsymbol{0}_{2\times 1} & \boldsymbol{0}_{2\times 5} \\ \boldsymbol{A}_{41} & \boldsymbol{0}_{2\times n} & \boldsymbol{A}_{43} & \boldsymbol{A}_{44} & \boldsymbol{A}_{45} & \boldsymbol{0}_{2\times 5} \\ \boldsymbol{A}_{51} & \boldsymbol{A}_{52} & \boldsymbol{A}_{53} & \boldsymbol{A}_{54} & \boldsymbol{A}_{55} & \boldsymbol{A}_{56} \\ \boldsymbol{A}_{61} & \boldsymbol{0}_{n\times 5} & \boldsymbol{A}_{63} & \boldsymbol{A}_{64} & \boldsymbol{A}_{65} & \boldsymbol{A}_{66} \end{bmatrix}_{(2n+10)\times(2n+10)}$$

$$\boldsymbol{F} = \begin{Bmatrix} 0 \\ 0 \\ \vdots \\ 0 \\ \emptyset_1(x)(F_{mo} + Ck_z z_r) \\ \emptyset_2(x)(F_{mo} + Ck_z z_r) \\ \vdots \\ \emptyset_n(x)(F_{mo} + Ck_z z_r) \\ 0 \\ 0 \\ 0 \\ -C\dfrac{k_z}{m_b} z_r \\ -D\dfrac{k_z}{k_i}\dot{z}_r - EC\dfrac{k_1 k_z}{L_0 m_b} z_r \\ 0 \\ \dfrac{-k_z C}{m_b T_1} z_r \\ 0 \\ \dfrac{z_r}{T_4} \\ 0 \end{Bmatrix}_{(2n+10)\times 1}$$

$$\boldsymbol{A}_{bb} = \begin{bmatrix} \boldsymbol{0}_{n\times n} & \boldsymbol{I}_{n\times n} \\ \boldsymbol{A}_{21} & \boldsymbol{A}_{22} \end{bmatrix}, \boldsymbol{A}_{bv} = \begin{bmatrix} \boldsymbol{0}_{n\times 2} & \boldsymbol{0}_{n\times 2} \\ \boldsymbol{A}_{23} & \boldsymbol{0}_{n\times 2} \end{bmatrix}, \boldsymbol{A}_{bi} = \begin{bmatrix} \boldsymbol{0}_{n\times 1} \\ \boldsymbol{A}_{25} \end{bmatrix}, \boldsymbol{A}_{b\tilde{x}} = \begin{bmatrix} \boldsymbol{0}_{n\times 5} \\ \boldsymbol{0}_{n\times 5} \end{bmatrix}, \boldsymbol{A}_{vb} = \begin{bmatrix} \boldsymbol{0}_{2\times n} & \boldsymbol{0}_{2\times n} \\ \boldsymbol{A}_{41} & \boldsymbol{0}_{2\times n} \end{bmatrix}, \boldsymbol{A}_{vv} = \begin{bmatrix} \boldsymbol{0}_{2\times 2} & \boldsymbol{I}_{2\times 2} \\ \boldsymbol{A}_{43} & \boldsymbol{A}_{44} \end{bmatrix}, \boldsymbol{A}_{vi} = \begin{bmatrix} \boldsymbol{0}_{2\times 1} \\ \boldsymbol{A}_{45} \end{bmatrix}, \boldsymbol{A}_{v\tilde{x}} = \begin{bmatrix} \boldsymbol{0}_{2\times 5} \\ \boldsymbol{0}_{2\times 5} \end{bmatrix}$$

$$\boldsymbol{A}_{ib} = [\boldsymbol{A}_{51} \quad \boldsymbol{A}_{52}], \boldsymbol{A}_{iv} = [\boldsymbol{A}_{53} \quad \boldsymbol{A}_{54}], \boldsymbol{A}_{ii} = [\boldsymbol{A}_{55}], \boldsymbol{A}_{i\tilde{x}} = [\boldsymbol{A}_{56}], \boldsymbol{A}_{\tilde{x}b} = [\boldsymbol{A}_{61} \quad \boldsymbol{0}_{n\times 5}], \boldsymbol{A}_{\tilde{x}v} = [\boldsymbol{A}_{63} \quad \boldsymbol{A}_{64}], \boldsymbol{A}_{\tilde{x}i} = [\boldsymbol{A}_{65}], \boldsymbol{A}_{\tilde{x}\tilde{x}} = [\boldsymbol{A}_{66}]$$

$$\boldsymbol{A}_{21} = \begin{bmatrix} -\omega_1^2 & & 0 \\ & \ddots & \\ 0 & & -\omega_n^2 \end{bmatrix}_{n\times n} + k_z C \begin{bmatrix} \emptyset_1^2(x) & \emptyset_1(x)\emptyset_2(x) & \cdots & \cdots & \emptyset_1(x)\emptyset_n(x) \\ \emptyset_2(x)\emptyset_1(x) & \emptyset_2^2(x) & \cdots & \cdots & \emptyset_2(x)\emptyset_n(x) \\ \vdots & & \ddots & & \vdots \\ \vdots & & & & \vdots \\ \emptyset_n(x)\emptyset_1(x) & \emptyset_n(x)\emptyset_2(x) & & & \emptyset_n^2(x) \end{bmatrix}_{n\times n}, \quad \boldsymbol{A}_{22} = \begin{bmatrix} -2\xi_1\omega_1 & & 0 \\ & \ddots & \\ 0 & & -2\xi_n\omega_n \end{bmatrix}_{n\times n}$$

$$\boldsymbol{A}_{23} = -k_z C \begin{bmatrix} 0 & \emptyset_1(x) \\ 0 & \emptyset_2(x) \\ \vdots & \vdots \\ 0 & \emptyset_n(x) \end{bmatrix}_{n\times 2}, \quad \boldsymbol{A}_{25} = k_i B \begin{bmatrix} \emptyset_1(x) \\ \emptyset_2(x) \\ \vdots \\ \emptyset_n(x) \end{bmatrix}_{n\times 1}, \boldsymbol{A}_{41} = k_z C \begin{bmatrix} 0 & 0 & \cdots & 0 \\ -\emptyset_1(x)/m_b & -\emptyset_2(x)/m_b & \cdots & -\emptyset_n(x)/m_b \end{bmatrix}_{2\times n}$$

$$\boldsymbol{A}_{43} = k_s \begin{bmatrix} -\dfrac{1}{m_c} & \dfrac{1}{m_c} \\ \dfrac{1}{m_b} & -\dfrac{1}{m_b} + \dfrac{k_z}{k_s m_b} C \end{bmatrix}_{2\times 2}, \boldsymbol{A}_{44} = c_s \begin{bmatrix} -\dfrac{1}{m_c} & \dfrac{1}{m_c} \\ \dfrac{1}{m_b} & -\dfrac{1}{m_b} \end{bmatrix}_{2\times 2}, \boldsymbol{A}_{45} = \boldsymbol{B} \begin{bmatrix} 0 \\ -\dfrac{k_i}{m_b} \end{bmatrix}_{2\times 1}, \boldsymbol{A}_{52} = D \begin{bmatrix} -\dfrac{k_z}{k_i}\emptyset_1(x) & -\dfrac{k_z}{k_i}\emptyset_2(x) & \cdots & -\dfrac{k_z}{k_i}\emptyset_n(x) \end{bmatrix}_{1\times n}$$

$$\boldsymbol{A}_{51} = \left[-D\frac{k_z}{k_i} V\emptyset_1'(x) - EC\frac{k_z k_1}{L_0 m_b}\emptyset_1(x) \quad -D\frac{k_z}{k_i} V\emptyset_2'(x) - EC\frac{k_z k_1}{L_0 m_b}\emptyset_2(x) \quad \cdots \quad -D\frac{k_z}{k_i} V\emptyset_n'(x) - EC\frac{k_z k_1}{L_0 m_b}\emptyset_n(x) \right]_{1\times n}$$

$$\boldsymbol{A}_{53} = E\left[\frac{k_s k_1}{L_0 m_b} \quad \frac{(k_z C - k_s)k_1}{L_0 m_b}\right]_{1\times 2}, \boldsymbol{A}_{54} = \left[E\frac{c_s k_1}{L_0 m_b} \quad D\frac{k_z}{k_i} - E\frac{c_s k_1}{L_0 m_b}\right]_{1\times 2}, \boldsymbol{A}_{55} = E\left[-\frac{R}{L_0} - \frac{k_i B k_1}{L_0 m_b}\right]_{1\times 1}, \boldsymbol{A}_{56} = E\left[-\frac{k_1}{L_0} \quad \frac{k_2 - k_1 V_1}{L_0} \quad \frac{k_3}{L_0} \quad \frac{k_4 + k_1 V_1}{L_0} \quad \frac{k_5}{L_0}\right]_{1\times 5}$$

$$\boldsymbol{A}_{61} = \begin{bmatrix} 0 & 0 & \cdots & \cdots & 0 \\ \dfrac{k_z C\emptyset_1(x)}{m_b T_1} & \dfrac{k_z C\emptyset_2(x)}{m_b T_1} & \cdots & \cdots & \dfrac{k_z C\emptyset_5(x)}{m_b T_1} \\ 0 & 0 & \cdots & \cdots & 0 \\ \dfrac{\emptyset_1(x)}{T_4} & \dfrac{\emptyset_2(x)}{T_4} & \cdots & \cdots & \dfrac{\emptyset_5(x)}{T_4} \\ 0 & 0 & \cdots & \cdots & 0 \end{bmatrix}_{5\times n}$$

$$\boldsymbol{A}_{63} = \begin{bmatrix} 0 & 0 \\ \dfrac{k_s}{m_b T_1} & \dfrac{k_z C - k_s}{m_b T_1} \\ 0 & 0 \\ 0 & 0 \\ 0 & 0 \end{bmatrix}_{2\times 5}, \quad \boldsymbol{A}_{64} = \begin{bmatrix} 0 & 0 \\ \dfrac{c_s}{m_b T_1} & \dfrac{-c_s}{m_b T_1} \\ 0 & 0 \\ 0 & 0 \\ 0 & 0 \end{bmatrix}_{2\times 5}, \quad \boldsymbol{A}_{65} = \begin{bmatrix} 0 \\ \dfrac{-k_i B}{m_b T_1} \\ 0 \\ 0 \\ 0 \end{bmatrix}_{1\times 5}, \quad \boldsymbol{A}_{66} = \begin{bmatrix} 0 & \dfrac{1}{T_3} & 0 & \dfrac{-1}{T_3} & 0 \\ \dfrac{-1}{T_1} & \dfrac{-V_1}{T_3} & 0 & \dfrac{V_1}{T_1} & 0 \\ 0 & \dfrac{1}{T_2} & \dfrac{-V_2}{T_2} & 0 & \dfrac{V_2}{T_2} \\ 0 & 0 & 0 & \dfrac{-V_3}{T_4} & \dfrac{-1}{T_4} \\ 0 & 0 & 0 & \dfrac{1}{T_5} & 0 \end{bmatrix}_{5\times 5}$$